ACS OMEGA

Open Access

http://pubs.acs.org/journal/acsodf

Article

Temperature Cycling Induced Deracemization of *p*-Synephrine in the Presence of Degradation

Po Sang Lo, Madiha Nisar, and Richard Lakerveld*

Cite This: *ACS Omega* 2024, 9, 41936−41943

Read Online

ACCESS | Metrics & More | Article Recommendations | Supporting Information

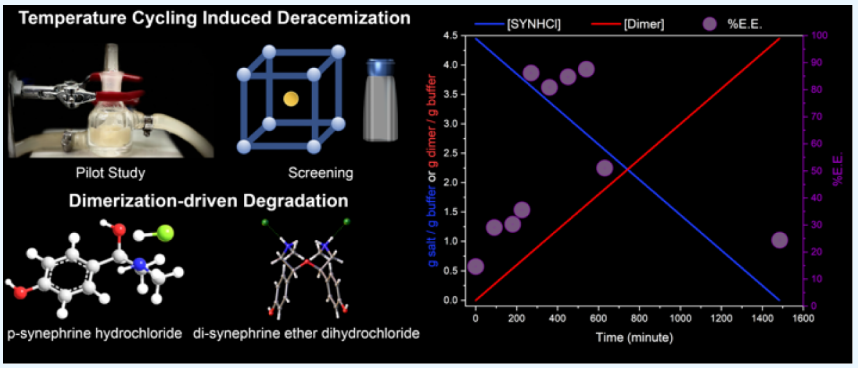

ABSTRACT: The acquisition of enantioenriched organic molecules is crucial in processes where the enantiomeric purity of active ingredients impacts efficacy and safety. Temperature cycling-induced deracemization (TCID) can achieve deracemization, but its effectiveness can be hindered by degradation reactions that influence the kinetics and the achievable enantioenrichment. This work characterizes the impact of degradation on the dynamic development of enantiomeric excess during the TCID process for the *p*-synephrine hydrochloride salt. The pilot study demonstrates that a maximum enantiomeric excess of 86% *R*-(-)-*p*-synephrine can be achieved at an intermediate batch time among all tested conditions. Degradation promoted the crystallization of a dimer with novel solid-state form, disynephrine ether dihydrochloride, which led to a substantial decrease in the slurry density of synephrine, potentially contributing to the observed decline in enantiomeric excess during the TCID process. Batch-to-batch variability in process dynamics and maximum attainable enantiomeric excess was observed, potentially attributable to the sensitivity of the process to uncontrolled initial conditions. These findings underscore the importance of accounting for degradation kinetics in the design and optimization of TCID processes for enantioenrichment.

1. INTRODUCTION

Enantiomeric separation is often crucial in the pharmaceutical industries,[1] as enantiomers can exhibit different biological activities,[2] necessitating the development of enantiopure drugs.[3,4] Viedma ripening, a chiral resolution method, deracemizes racemic mixtures into a single chirality by grinding the suspension with glass beads,[5] requiring an initial chiral imbalance, a conglomerate-forming solid-state system, and a racemization reaction in solution.[6] The performance of Viedma ripening is governed by kinetic phenomena, including the racemization reaction, agglomeration process, and crystal growth and dissolution.[7] Temperature cycle-induced deracemization (TCID) offers a more convenient and scalable alternative, utilizing temperature-dependent solubility to induce dissolution−recrystallization cycles.[8] TCID promotes deracemization by dissolving small crystals in heating phases and growing crystals in cooling phases.[9] This process can be explained by the crystal growth with chiral clusters[10] and the amplification of process asymmetries due to the nonlinear effect of temperature changes.[11] TCID has several advantages over Viedma ripening, including not requiring high attrition rates[12] and allowing good control over the final product configuration through seeding.[13] However, TCID may in general only reach completeness for a conglomerate system without partial solid solution[9] and is sensitive to initial conditions.[12] Nonstereoselective agglomeration can form racemic agglomerates during the TCID process, but secondary nucleation can counteract this and accelerate deracemization.[14,15]

Despite the potential for complete deracemization using Viedma ripening-based methods,[16] certain cases may not maintain or reach completeness.[15−19] These limitations can be

Received: July 24, 2024
Accepted: August 27, 2024
Published: September 27, 2024

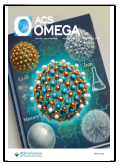

Scheme 1. Racemization Reaction Scheme of *R*-(-)-*p*-Synephrine in Acidic Media[25]

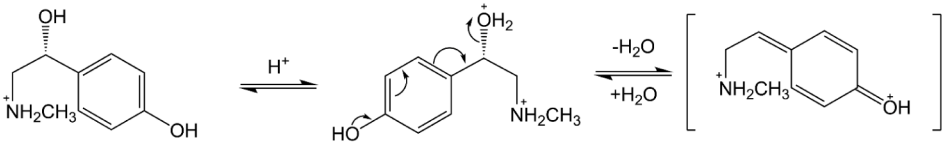

Scheme 2. Elimination Reaction to Form Di-Synephrine Ether Dihydrochloride (Dimer)

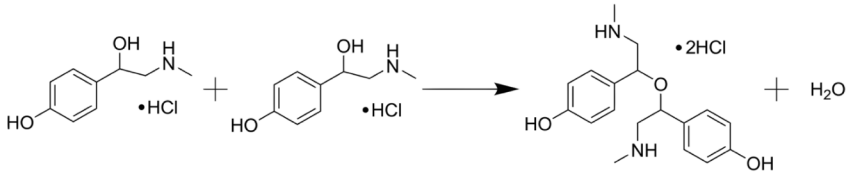

attributed to factors such as degradation at high temperatures,[20] occurring concurrently with racemization[8] during temperature cycling. Degradation can lead to lower yields, byproduct formation, and impurity incorporation during crystallization.[21] Given the prevalence of degradation for many active ingredients, characterizing the impact of degradation on the dynamic development of the enantiomeric excess during TCID for commercially attractive compounds is crucial. Notwithstanding the potential implications of degradation on dissolution and crystallization rates driving TCID, studies characterizing these phenomena for practical cases are lacking, with limited research examining degradation susceptibility of Viedma ripening-based deracemization.[22,23] The impact of degradation on the dynamic development of enantiomeric excess during the batch of a TCID process, such as the reduction of slurry density of the raw material or the crystallization of byproducts that may alter the solid composition in suspension, remains unexplored.

This study investigates the effect of degradation on the enantioenrichment process during TCID, using a *p*-synephrine hydrochloride salt as a model compound. *p*-Synephrine is an active ingredient in *Aurantii Fructus Immaturus*.[24] The biologically active *R*-(-)-*p*-synephrine enantiomer demonstrates higher pharmacological activity,[25] and enhancing its fraction can potentially increase effectiveness and reduce side effects.[26] Enantiomeric separation is necessary due to racemization in natural sources and manufactured synephrine-containing products,[25,27] but current chromatography methods result in yield losses exceeding 50%.[28] *p*-Synephrine freebase forms a stable racemic compound,[29,30] limiting Viedma ripening-based deracemization and hindering enantioenrichment without considerable loss. However, *p*-synephrine hydrochloride salt is expected to crystallize as a conglomerate due to differences in melting points between its racemate[31] and enantiomers,[32] suggesting the potential for TCID.[33] The racemization reaction scheme of *R*-(-)-*p*-synephrine in acidic media (Scheme 1)[25] indicates that acidic crystallization conditions can enhance racemization kinetics, potentially supporting deracemization of the hydrochloride salt.[34,35] The stable benzylic carbonium ion intermediate involved may also lead to degradation via competing reactions, such as dimerization to form disynephrine ether dihydrochloride through an elimination reaction (Scheme 2), as supported by the formation of a *p*-synephrine derivative dimer with bromine salt during crystallization.[36] Other potential degradation pathways, such as aziridine formation via ring closure of the benzylic carbonium ion, may also be possible. Consequently, the pH is expected to be an important factor and can potentially optimize the balance between deracemization and degradation rates.

The objectives of this study were to investigate the attainable enantioenrichment of *p*-synephrine hydrochloride salt using the TCID process and to evaluate the impact of degradation on deracemization efficiency. A pilot study was conducted in a 25 mL jacketed vessel to investigate the combined dynamics of the TCID process and degradation at a low pH, followed by two sets of design of experiments (DoE) in 1 mL vials to explore the potential for achieving higher enantiomeric excesses (ee) under less acidic conditions. The DoE study varied operating conditions, including temperature swing, heating rate, cooling rate, minimum temperature, and amount of seed crystals. To explore degradation events, synephrine depletion kinetics was monitored, and the solid-state form of the degradation byproduct was characterized, revealing the formation of a dimer with novel solid-state form. Synthesis of this dimer was analyzed to confirm that dimerization was the main degradation pathway. Multiple characterization techniques were employed, including high-performance liquid chromatography (HPLC), powder X-ray diffraction (PXRD), single-crystal X-ray diffraction (SC-XRD), differential scanning calorimetry (DSC), thermogravimetric analysis (TGA), and optical microscopy.

2. RESULTS AND DISCUSSION

2.1. Deracemization of *p*-Synephrine Hydrochloride Salt via the TCID Process. The pilot study (experiments PT-01 to PT-08 and PS-01 to PS-04) investigated the enantioenrichment of the synephrine hydrochloride salt using the TCID process. Experiment PT-03 achieved the highest enantioenrichment of 86% ee of *R*-(-)-synephrine at the sixth cycle (Figure 1). Attempts to obtain higher enantiomeric excess under less acidic conditions and different operating parameters through two sets of DoE did not exceed 50% ee after 24 h, likely due to slower racemization kinetics[34,35] (Supplementary Note 1F). To elucidate the process characteristics influencing dynamics and variability, experiments PS-01 to PS-04 examined the relationship between enantiomeric excess and solid-state properties during the TCID process (Figure 2). The observed increase in the melting point of the sampled solids (Figure 2B) with rising enantiomeric excess (Figure 2A) is consistent with the behavior of a conglomerate-forming system.[37] The possibility of *S*(+) enantiomer

https://doi.org/10.1021/acsomega.4c06807
ACS Omega 2024, 9, 41936−41943

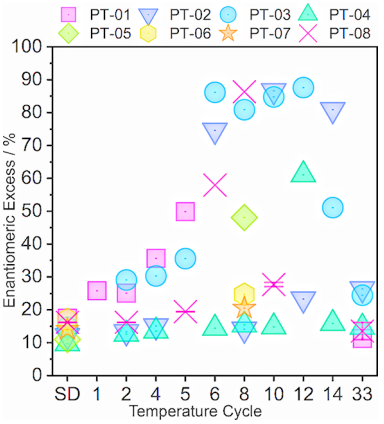

Figure 1. Dynamic development of the enantiomeric excess for pilot study experiments PT-01 to PT-08 (see Section 4.2 for experimental details). SD: initial enantiomeric excess, samples collected 10 min after enantiopure *R*-(-)-*p*-synephrine freebase addition.

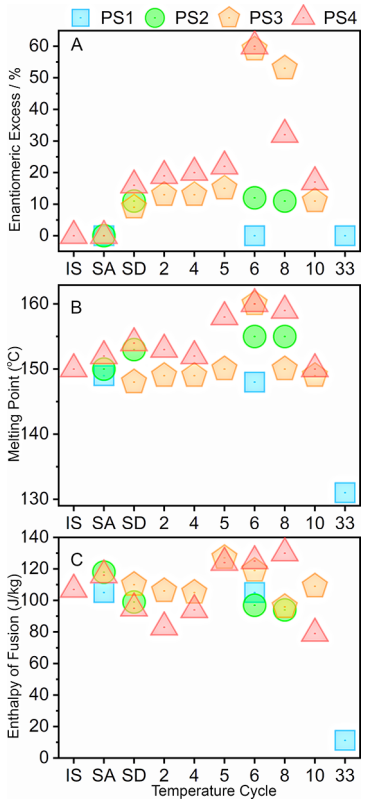

Figure 2. Dynamic development of the enantiomeric excess and solid-state forms for pilot study experiments PS-01 to PS-04 (see Section 4.2 for experimental details). (A) Enantiomeric excess. (B) Melting point. (C) Enthalpy of fusion. IS: RS-SYNHCl salt slurry; SA: RS-SYNHCl salt slurry resuspended with 0.5 mL of salt buffer solution ([3g of RS-SYNHCl salt]/[mL of 4 M HCl/KCl buffer]); SD: initial enantiomeric excess samples, collected 10 min post enantiopure *R*-(-)-*p*-synephrine freebase addition.

contamination in the *R*(−) enantiomer crystal may explain the difficulty in achieving complete deracemization. Furthermore, even under optimized conditions, inherent racemization during the TCID process can introduce the undesired enantiomer, thus preventing complete enantioenrichment. The pilot study results also demonstrated that prolonged processing led to a reduction in enantiomeric excess, emphasizing the importance of an optimal batch time for maximizing enantioenrichment (Figures 1 and 2A). Batch-to-batch variability in the maximum achievable enantiomeric excess and process dynamics was observed. This variability was unlikely to be caused by sampling and workup steps, as duplicate samples collected at the same cycle in experiment PT-08 exhibited an average standard deviation of only 0.47% ee (Figure 1). Instead, the observed variability is hypothesized to be attributed to the interplay of various kinetic processes, such as reaction kinetics, agglomeration, secondary nucleation, crystal growth, and dissolution, which may be sensitive to variations in initial system properties, including crystal size and shape distribution, which were not tightly controlled in this pilot study.

2.2. Degradation during the TCID Process. The prolonged TCID process in the pilot study resulted in a notable decrease in enantiomeric excess, likely due to synephrine degradation (Supporting Information, Note 2B). The depletion of synephrine concentration in a nearly saturated solution over 22 h at the highest cycling temperature of 50 °C indicated the occurrence of degradation (Figure 4B). The initial decrease in concentration suggested a synephrine depletion rate of about 1.8×10^{-5} moles of synephrine per gram of buffer per minute under nearly saturated conditions. The onset of primary nucleation of the solid degradation byproduct occurred at 1085 min (Figure 4A), corresponding to a synephrine depletion of approximately 7.4×10^{-3} moles of synephrine per gram of buffer. This induction time served as an approximate reference for degradation byproduct nucleation, given that factors such as the solution volume, stirring conditions, and the stochastic nature of nucleation affect this nucleation point as well.

Single-crystal X-ray diffraction (SC-XRD) analyses confirmed that the crystal structure of the solid degradation byproduct is a dimer with novel solid-state form. Supersaturated synephrine hydrochloride salt solutions were maintained at 20 °C (experiment SS-01) and 50 °C (experiment SS-02) for slow evaporative crystallization. SC-XRD analysis revealed that the crystal from experiment SS-01 conformed to the known pattern of *R*-(-) synephrine hydrochloride salt,[38] while the crystal formed at 50 °C exhibited a structure with novel solid-state form (Supplementary Table 2-1). The novel structure, grown in Olex2 software to illustrate the full molecule (Supplementary Figure 2-1), suggested the formation of disynephrine ether dihydrochloride (dimer), as explained by the elimination reaction outlined in Scheme 2. The dimer crystallized in a monoclinic I/2a system, indicating the formation of a racemic compound. Crystallographic analysis showed half a formula per asymmetric unit ($Z' = 0.5$) and a 2-fold axis through the molecule (Supplementary Table 2-1), which suggested that the dimer in this monoclinic I/2a crystal system likely existed in *R*,*R* and *S*,*S* configurations, with potential for a meso form exhibiting internal symmetry (*R*,*S* or *S*,*R*) existing in solution.

The powder X-ray diffraction (PXRD) pattern of the dimer was simulated by using the SC-XRD data. The simulated PXRD pattern of the dimer was then referenced to confirm the presence of the dimer in samples from the TCID process (Figure 3). The dimer indeed appeared during the prolonged TCID process, supported by the sample collected at the thirty-third cycle in experiment PS-01 (sample PS-01 33rd cycle, ~24 h). The PXRD pattern of the sample PS-01 33rd cycle resembled the simulated pattern of the dimer, albeit with low crystallinity, devoid of characteristic peaks of synephrine

https://doi.org/10.1021/acsomega.4c06807
ACS Omega 2024, 9, 41936−41943

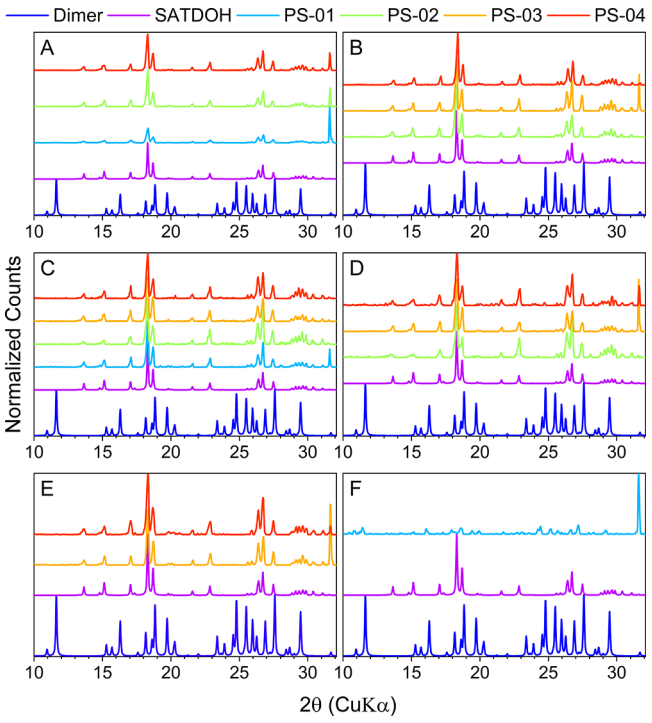

Figure 3. PXRD diagrams from pilot study experiments PS-01 to PS-04 (see Section 4.2 for experimental details). The sample collected (A) immediately after resuspending the RS-SYNHCl salt slurry with 0.5 mL RS-SYNHCl salt buffer solution ([3g RS-SYNHCl salt]/[mL 4 M HCl/KCl buffer]), (B) at 10 min after adding enantiopure *R*-(-)-*p*-synephrine freebase, and (C−F) immediately after completing the sixth, eighth, and tenth cycles and thirty-third cycle (~24 h), respectively. SATDOH: simulated PXRD pattern derived from *R*-(-)-*p*-synephrine hydrochloride salt.[38] Dimer: simulated PXRD pattern of disynephrine ether dihydrochloride from the SC-XRD data (Sections 4.3.2 and 4.4.4).

hydrochloride salt (Figure 3F). This sample also exhibited changes in melting temperature (Figure 2B) and enthalpy of fusion (Figure 2C). The DSC thermogram of the initial synephrine hydrochloride salt slurry (sample PS-01 SA) matched the raw material, while that of the sample PS-01 33rd cycle exhibited a broad, featureless endothermic transition (Supplementary Figure 2-6). Although the absence of clear endothermic transitions in the DSC melting point and enthalpy of fusion data for the sample PS-01 33rd cycle necessitated cautious interpretation (Figure 2B,C), such a DSC pattern resembled the dimer reference. Collectively, the data suggested substantial dimer formation, which coincided with the loss of enantiomeric enrichment following the prolonged TCID process.

Mass balance analysis identified dimer formation as the primary degradation pathway during the TCID process (Supporting Information, Note 2A). A supersaturated solution of synephrine hydrochloride salt, prepared by dissolving 40.5 g of synephrine hydrochloride salt in 10 mL of 4 M HCl/KCl buffer and maintained at 50 °C, resulted in 34.6 g of solid after 24 h. Subsequent PXRD analysis revealed that the crystal pattern of this solid was consistent with the simulated PXRD pattern of the dimer, indicating a predominant dimer composition (Supplementary Figure 2-2). Considering the solubility of the dimer at 50 °C, approximately 2.83 g of dimer was expected to remain dissolved. The total dimer yield, comprising both collected solid and dissolved fractions, amounted to 97% of the theoretical yield based on the proposed elimination reaction mechanism (Scheme 2). The discrepancy between input and output masses matched the solubility of synephrine hydrochloride salt at 50 °C. These results indicated the absence of other solid byproducts and implied that the solution mainly consisted of the dimer and synephrine, corroborating dimerization as the main degradation pathway during the TCID process.

2.3. Impact of Concurrent Dimerization on Deracemization Efficiency in the TCID Process. The formation and eventual crystallization of the dimer during the TCID process could affect the deracemization of *p*-synephrine in two possible ways. First, the degradation reaction could decrease the slurry density of synephrine due to dissolution, potentially impeding deracemization and reducing enantioenrichment provided that sufficiently rapid degradation occurred during the batch. Second, the solid dimer might influence secondary nucleation kinetics of the solid synephrine, modulating the deracemization rate, if substantial nucleation and growth of the solid dimer coincided with the decrease in enantiomeric excess.

To investigate these potential mechanisms, the dimer formation rate and its crystallization tendency were characterized. Dimerization emerged as the primary degradation pathway during the TCID process. Consequently, the synephrine depletion rate was postulated to correspond to the dimer formation rate, estimated at 0.003 g of dimer per gram of buffer per minute (Supplementary Note 2B). Furthermore, the synephrine concentration depleted for degradation was conjectured to be equivalent to the dimer concentration necessary for initiating the primary nucleation, approximately 1.44 g of dimer per gram of 4 M HCl/KCl buffer (Supplementary Note 2B), which is quintuple the dimer solubility at 50 °C (Supplementary Figure 2-7). Material balances were then employed to estimate the composition changes in the solution and solid phases during the batch. It was assumed that a saturated solution with respect to synephrine hydrochloride salt remained throughout due to faster dissolution compared to degradation and that no other side reactions occurred. Although the dimer formation rate was expected to decrease after complete synephrine dissolution and potential side reactions may have lowered this rate, these assumptions led to a constant dimer formation rate, which provided an upper limit estimation for the total dimer amount. The estimated overall composition changes were compared to the dynamic development of the enantiomeric excess of the synephrine hydrochloride salt (Supplementary Figure 2-9). This analysis revealed that the total dimer concentration surpassed the metastable zone limit for primary nucleation after 480 min, while the total synephrine hydrochloride salt amount reached its solubility limit at 40 °C by 713 min. The absence of substantial dimer in the earlier stages (Figure 3A−E) suggests that solid dimer interference was not a primary factor in the ee decline during the second half of the TCID process. However, the dimer formation rate and synephrine hydrochloride salt solubility (Supplementary Note 2B) indicated that around 40% of the initial synephrine hydrochloride salt mass had dissolved at the time of maximum enantiomeric excess, potentially impeding deracemization and contributing to the observed ee decline due to the reduced availability of synephrine in the solid phase for enantioenrichment.

https://doi.org/10.1021/acsomega.4c06807
ACS Omega 2024, 9, 41936−41943

3. CONCLUSION

This study characterized the impact of degradation on the dynamic development of enantiomeric excess during a TCID process for the *p*-synephrine hydrochloride salt. The TCID process achieved a maximum enantiomeric excess of 86% *R*-(-)-*p*-synephrine at an intermediate batch time. Increasing the pH level during the TCID process did not enhance enantioenrichment, as the expected decrease in the degradation rate may have been counterbalanced by a reduction in the racemization rate, highlighting the trade-offs in optimizing the TCID process. Batch-to-batch variability in process dynamics and maximum enantiomeric excess was observed, emphasizing the potential sensitivity of the process to uncontrolled initial conditions. Dimerization was identified as the main degradation pathway for the decrease in the enantiomeric excess following prolonged TCID processing. The crystallization of a dimer with novel solid-state form, disynephrine ether dihydrochloride, was confirmed by single-crystal X-ray diffraction and identified as the main degradation byproduct during the TCID process through mass balance analysis. The impact of dimerization on the deracemization efficiency was investigated by characterizing the dimer formation rate and its crystallization tendency. While the estimated mass fraction of the solid dimer was considered insufficient to substantially alter the attrition kinetics, the reduction in slurry density due to dimer formation potentially impeded deracemization and contributed to the observed decline in enantiomeric excess.

This study highlights several avenues for future research. First, implementing process analytical tools for monitoring solid-state properties or solution concentrations can potentially enhance throughput by enabling an optimal batch time or detect batch-to-batch variability early by measuring crystal properties not explored in this work, such as the crystal size distribution. Second, developing systematic methods for identifying a broader design space of the TCID process is essential, which could involve incorporating process modeling tools, constructing a phase diagram for *p*-synephrine hydrochloride salts, determining partial solid solutions between (−) and (+) *p*-synephrine hydrochloride salts, and exploring alternative solvent/buffer conditions. Third, intensifying the deracemization rate through techniques such as rapid temperature cycling in a continuous flow crystallizer with ultrasounds may mitigate the impact of degradation. Furthermore, determining the scalability of the reactions, exploring the deracemization performance using alternative methods such as diastereomeric resolution or Viedma ripening at lower temperatures, possibly in combination with TCID, and applying low-temperature recrystallization under minimal acidic conditions are potential directions to mitigate dimerization while recovering a product with high enantiomeric excess. Generally, elucidating the mechanisms, kinetics, and optimization of the dimerization process and its competing reactions is vital for the comprehensive optimization of the system. Finally, examining the effect of uncontrolled crystal attributes, such as particle size, on the deracemization process may provide new insights into the process dynamics and enable further optimization.

4. MATERIALS AND METHODS

4.1. Materials. Analytical grade chemicals and solvents were used as received. RS-(±)-*p*-synephrine hydrochloride salt (RS-SYNHCl salt, purity ≥ 98%), RS-(±)-*p*-synephrine freebase (purity ≥ 98%), and *R*-(-)-*p*-synephrine freebase (purity ≥ 98%) were obtained from Highassay (China), Sigma (USA), and TCI (Japan), respectively. Hydrochloric acid solution (HCl acid, 37% w/w, density: 1.2 g/mL) was purchased from Honeywell (Austria). DDI water was purified using a Milli-Q system (Millipore). 0.2 M HCl/KCl buffer (pH 1) was prepared by combining 40.70 mL of 0.2 M HCl acid, 9.30 mL of 0.2 M KCl solution, and 50 mL of DDI water. 4 M HCl/KCl buffer (pH 0.14) was prepared by mixing 40.70 mL of 4 M HCl acid, 9.30 mL of 4 M KCl solution, and 50 mL of DDI water. The HPLC mobile phase consisted of a 10 mM sodium phosphate buffer (pH 6.0) and 2-propanol mixture (95:5,w/w), with 50 μM disodium EDTA.[25]

4.2. Temperature Cycling-Induced Deracemization Experiment. The racemization kinetics of *R*-(-)-*p*-synephrine was determined, revealing a half-time of approximately one hour in a 4 M HCl/KCl buffer at 40 °C, typical for the TCID process[34,35] (Supplementary Note 1A). Preliminary experiments (A-01, A-02, and A-03) assessed TCID feasibility, with A-02 achieving ∼30% ee and showing an increasing trend (Supplementary Note 1B). These results informed the design of the pilot study. For the pilot study, RS-SYNHCl salt slurry was prepared by dissolving 4.05 g RS-SYNHCl salt in 1 mL 4 M HCl/KCl buffer in a 25 mL jacketed vessel, heating to 70 °C for 15 min with 300 rpm magnetic stirring, and then cooling to room temperature to induce crystallization (Supplementary Note 1C). The temperature was regulated by a thermostatic bath (PolyScience AP07R-20-A12P). Due to limited control over solid content, the suspension was filtered, and the residue (∼20% buffer) was collected. In the TCID process, 5.2 g collected RS-SYNHCl salt slurry was resuspended in 0.5 mL RS-SYNHCl salt buffer solution ([3 g RS-SYNHCl salt]/[mL 4 M HCl/KCl buffer]) in a 25 mL of jacketed vessel and stirred at 300 rpm for 10 min at 40 °C. To induce initial enantiomeric excess, 300 mg enantiopure *R*-(-)-*p*-synephrine freebase was added, rapidly converting to the salt under the acidic conditions[39] (Supplementary Note 1D). The temperature cycling profile ranged between 40 and 50 °C with a heating rate of 1.75 °C/min, a cooling rate of 0.55 °C/min, and a hold time of 10 min at each temperature extreme (Supplementary Note 1E). Twelve experiments (PT-01 to PT-08 and PS-01 to PS-04) investigated the effect of varying the total number of temperature cycles. PT-01, PT-02, PT-03, PT-04, PT-08, and PS-01 underwent 33 cycles (∼24 h). PT-05, PT-06, PT-07, and PS-02 were exposed to 8 cycles. PS-03 and PS-04 experienced 10 cycles. The collected samples were filtered, washed, and dried in a vacuum oven and characterized for ee of the dried solid. PXRD and DSC were used to analyze the solid-state forms of samples from experiments PS-01 to PS-04. Furthermore, two DoE screening studies using a one-milliliter parallel crystallization system (Crystal 16, Technobis) investigated the feasibility of achieving a higher ee under less acidic conditions (0.2 M HCl/KCl buffer) and different operating conditions not controlled in the pilot study (Supplementary Note 1F). The investigated factors included temperature swing, heating rate, cooling rate, minimum temperature, and the amount of seed crystals.

4.3. Degradation Experiment. *4.3.1. Synephrine Depletion Kinetics at 50 °C.* To evaluate the stability of synephrine during the TCID process, the depletion kinetics was monitored at the highest cycling temperature of 50 °C. A nearly saturated solution containing 30 g of RS-SYNHCl in 10 mL of the buffer was prepared in a temperature-controlled

https://doi.org/10.1021/acsomega.4c06807
ACS Omega 2024, 9, 41936−41943

jacketed vessel. Complete dissolution was achieved at 58 °C with magnetic stirring at 300 rpm for 15 min, as evidenced by 100% transmission recorded by Crystal 16 (Figure 4A).

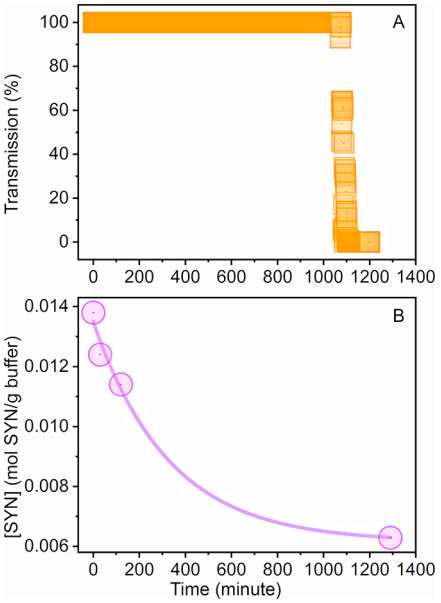

Figure 4. Synephrine depletion kinetics at 50 °C (see Section 4.3.1; Supporting Information, Note 2B). The concentration of *p*-synephrine hydrochloride salt buffer solution was 3g of RS-SYNHCl salt per mL of 4 M HCl/KCl buffer. The temperature was 50 °C. (A) Transmission recorded in Crystal 16. (B) Synephrine concentration measured by HPLC over time.

Subsequently, the solution was consistently maintained at 50 °C, and 1 mL of aliquots was sampled at various time intervals. These samples were filtered through a 0.22 μm filter, diluted with an HPLC mobile phase, and analyzed by HPLC to quantify synephrine concentrations (Supplementary Note 2B). The induction time for solid byproduct nucleation was also measured by Crystal 16 (Figure 4A).

4.3.2. Solid-State Form Analysis for Degradation Byproducts. Following the observation of synephrine degradation at 50 °C (Section 4.3.1), the solid-state form of the degradation byproducts was characterized using SC-XRD. A supersaturated solution containing 8.1 g of RS-SYNHCl salt in 2 mL of 4 M HCl/KCl buffer was prepared at 70 °C with 300 rpm magnetic stirring for 15 min. The supersaturated solution underwent slow evaporation crystallization in a temperature-regulated jacketed vessel at either 20 °C (experiment SS-01) or 50 °C (experiment SS-02). Crystals suitable for SC-XRD analysis were obtained after one day at 20 °C and three days at 50 °C.

4.3.3. Dimer Synthesis and Characterization. Upon confirmation of dimer formation from synephrine degradation (Section 4.3.2), the hypothesis that dimerization is the primary degradation pathway was investigated, and the physical properties of the dimer were assessed. A targeted synthesis of the dimer was conducted based on the conditions outlined in Section 4.3.2. A supersaturated RS-SYNHCl salt solution was prepared by dissolving 40.5 g of the salt in 10 mL of 4 M HCl/KCl buffer at 70 °C with continuous stirring at 300 rpm for 15 min. This solution was then maintained at 50 °C for 24 h with continuous stirring to facilitate the dimer formation. The resultant solid dimer was collected, dried under vacuum at room temperature for 24 h to remove solvents, and characterized using PXRD, DSC, TGA, and optical microscopy. Solubility was examined using the clear point method with Crystal 16. A quantity of 0.1 to 0.6 g of the dried dimer was added to 1 mL of 4 M HCl/KCl buffer and stirred at 20 °C for 15 min. The mixture was subsequently heated to 80 °C at a rate of 0.2 °C/min with 700 rpm magnetic stirring. The clear point was recorded as the temperature at which the solution became completely transparent. The yield of dimer formation was quantified using the mass balance method, to determine if dimerization was the dominant degradation pathway.

4.4. Characterization. *4.4.1. Differential Scanning Calorimetry (DSC).* Thermal properties were analyzed using a TA Q1000 DSC system (TA System, USA). Samples (1−5 mg) were hermetically sealed in aluminum pans and heated from 25 to 220 °C at 10 °C/min under a nitrogen purge gas flow. Thermal data were recorded and processed using Advantage Software v5.5.24, and the resulting DSC thermograms are provided in Supplementary Data 2.

4.4.2. High-Performance Liquid Chromatography (HPLC). Enantiomeric excess of *R*-(-)-*p*-synephrine was quantified following the HPLC method of Pellati et al.[25] Separation used a Chiral-CBH column (100 × 4.0 mm i.d., 5 μm, ChromTech, Congleton, UK) with a guard column (10 × 4.0 mm, 5 μm) under isocratic elution (20 °C, 0.8 mL/min flow rate, 5 μL injection volume, 225 nm detection wavelength) for a total analysis time of 10 min. HPLC samples were prepared by dissolving 10 mg of dried solid in 10 mL of DDI water, stirring at 300 rpm for 15 min at 20 °C, and filtering through a 0.22 μm filter. A 50 μL aliquot of the filtrate was diluted with 950 μL of the mobile phase to obtain the HPLC sample. Retention times for *R*-(-)-*p*-synephrine and S-(+)-*p*-synephrine were approximately 2.5 and 3.2 min, respectively. Peak areas (AU*minutes) of the HPLC chromatograms were analyzed using Empower 2 software (USA) (Supplementary Data 1), and the percentage of enantiomeric excess for *R*-(-)-*p*-synephrine was calculated using eq :1

$$\%E.\,E. = \frac{S_R - S_S}{S_R + S_S} \times 100\% \quad (1)$$

where % ee is the percentage of enantiomeric excess for *R*-(-)-*p*-synephrine enantiomer. S_R is the peak area of the *R*-(-)-*p*-synephrine enantiomer. S_S is the peak area of *S*-(+)-*p*-synephrine enantiomer.

4.4.3. Powder X-ray Diffraction (PXRD). Finely ground solid samples were analyzed at ambient temperature using a PANalytical X'Pert Pro diffractometer with Cu Kα radiation (λ=1.54056Å, 40kV, 40mA) over a scan range of 4 ° to 60 ° with a step size of 0.033 °. Diffraction patterns were processed by applying background subtraction, smoothing, and 0.05 ° to 0.105 ° displacement corrections. The simulated PXRD pattern of the dimer from SCXRD data was performed by Mercury 4.0 software[40] (Cambridge Crystallographic Data Centre Inc., USA).

4.4.4. Single Crystal X-ray Diffraction (SC-XRD). Data was collected at 100 K on a Rigaku-Oxford Diffraction Supernova diffractometer equipped with a microfocus Cu Kα source and Atlas detector. The structure was solved by the charge flipping algorithm (Olex-solve)[41,42] and refined with SHELXL.[43] Refinement restraints were set up within the Olex2 software package,[44] which was also used to prepare crystallographic

https://doi.org/10.1021/acsomega.4c06807
ACS Omega 2024, 9, 41936−41943

figures. Nonhydrogen atoms were refined anisotropically, while hydrogen atoms bonded to carbon were placed geometrically and handled with riding constraints. The high degree of agreement between the structure suggested by Olex2 and the collected SCXRD data, as evidenced by the low *R*-factor values approaching to zero,[45] supports the structure determination of the dimer with novel solid-state form.

4.4.5. Thermogravimetric Analysis (TGA). Thermal degradation was investigated by using a TA Q500 instrument (TA System, USA). Samples (1−5 mg) in aluminum pans were heated from 25 to 800 °C at 10 °C/min under nitrogen. Sample weight was continuously monitored as a function of temperature, and thermogravimetric data were processed using Advantage Software v5.5.24.

4.4.6. Optical Microscope. Dimer morphology was examined by using an optical microscope (Eclipse Ni-U, Nikon) with a digital camera (Digital Sight Qi2, Nikon). A 1 mL suspension aliquot was withdrawn from a jacketed vessel by syringe (Terumo, 1 mL), dispensed onto a glass slide (Sail, ground edges, 1 × 3 in.), and covered with a glass cover (Marienfeld, 22 mm × 22 mm). Images were acquired at room temperature using a 20× objective (536 × 536 pixels, 16-bit depth).

■ ASSOCIATED CONTENT

Supporting Information

The Supporting Information is available free of charge at https://pubs.acs.org/doi/10.1021/acsomega.4c06807.

Supplementary Note 1: temperature cycling-induced deracemization, Supplementary Note 2: dimerization-driven degradation, Supplementary Data 1: HPLC chromatograms for pilot study experiments, and Supplementary Data 2: DSC thermograms for pilot study experiments (PDF)

■ AUTHOR INFORMATION

Corresponding Author

Richard Lakerveld − *Department of Chemical and Biological Engineering, The Hong Kong University of Science and Technology, Kowloon, Hong Kong, China;* orcid.org/0000-0001-7444-2678; Email: r.lakerveld@ust.hk

Authors

Po Sang Lo − *Department of Chemical and Biological Engineering, The Hong Kong University of Science and Technology, Kowloon, Hong Kong, China;* orcid.org/0000-0001-7835-5248

Madiha Nisar − *Department of Chemical and Biological Engineering, The Hong Kong University of Science and Technology, Kowloon, Hong Kong, China; Department of Chemistry, The Hong Kong University of Science and Technology, Kowloon, Hong Kong, China;* Present Address: Baxter Laboratories, Melbourne VIC 3155, Australia

Complete contact information is available at: https://pubs.acs.org/10.1021/acsomega.4c06807

Author Contributions

The manuscript was written through contributions of all authors. All authors have given approval to the final version of the manuscript.

Notes

The authors declare no competing financial interest.

■ ACKNOWLEDGMENTS

The authors wish to extend their appreciation to Miss Carrie W Y Law, Miss Yi Chen Wu, and Miss Christine P Y Cheung from the Materials Characterization and Preparation Facility (MCPF(CWB)) at the Hong Kong University of Science and Technology for their assistance with DSC, TGA, and PXRD. Additional thanks are due to Mr. Kam Tim Tang of the Department of Chemical and Biological Engineering at the Hong Kong University of Science and Technology for his assistance with HPLC.

■ ABBREVIATIONS

TCID: temperature cycling-induced deracemization; DoE: design of experiment; HPLC: high-performance liquid chromatography; PXRD: powder X-ray diffraction; SC-XRD: single-crystal X-ray diffraction; DSC: differential scanning calorimetry; TGA: thermogravimetric analysis; RS-SYNHCl salt: racemic *p*-synephrine hydrochloride salt; ee: enantiomeric excess; Dimer: disynephrine ether dihydrochloride

■ REFERENCES

(1) Collins, A. N.; Sheldrake, G.; Crosby, J. *Chirality in industry II: developments in the commercial manufacture and applications of optically active compounds*; John Wiley & Sons, 1998.

(2) Nguyen, A. L.; He, H.; Pham-Huy, C. Chiral Drugs: An Overview. *Int. J. Biomed. Sci.* **2006**, *2* (2), 85−100.

(3) Brooks, W. H.; Guida, W. C.; Daniel, K. G. The significance of chirality in drug design and development. *Curr. Top. Med. Chem.* **2011**, *11* (7), 760−770.

(4) Center for Drug Evaluation and Research *Guidance Document Development of New Stereoisomeric Drugs*; U.S. Food and Drug Administration, 1992. https://www.fda.gov/regulatory-information/search-fda-guidance-documents/development-new-stereoisomeric-drugs. accessed June 2022.

(5) Viedma, C. Chiral symmetry breaking during crystallization: complete chiral purity induced by nonlinear autocatalysis and recycling. *Phys. Rev. Lett.* **2005**, *94* (6), 065504.

(6) Sögütoglu, L.-C.; Steendam, R. R.; Meekes, H.; Vlieg, E.; Rutjes, F. P. Viedma ripening: a reliable crystallisation method to reach single chirality. *Chem. Soc. Rev.* **2015**, *44* (19), 6723−6732.

(7) Iggland, M.; Mazzotti, M. A population balance model for chiral resolution via Viedma ripening. *Cryst. Growth Des.* **2011**, *11* (10), 4611−4622.

(8) Intaraboonrod, K.; Lerdwiriyanupap, T.; Hoquante, M.; Coquerel, G.; Flood, A. E. Temperature cycle induced deracemization. *Mendeleev Commun.* **2020**, *30* (4), 395−405.

(9) Suwannasang, K.; Flood, A.; Rougeot, C.; Coquerel, G. Using programmed heating−cooling cycles with racemization in solution for complete symmetry breaking of a conglomerate forming system. *Cryst. Growth Des.* **2013**, *13* (8), 3498−3504.

(10) Uchin, R.; Suwannasang, K.; Flood, A. E. Model of Temperature Cycle-Induced Deracemization via Differences in Crystal Growth Rate Dispersion. *Chem. Eng. Technol.* **2017**, *40* (7), 1252−1260.

(11) Bodák, B.; Maggioni, G. M.; Mazzotti, M. Population-based mathematical model of solid-state deracemization via temperature cycles. *Cryst. Growth Des.* **2018**, *18* (11), 7122−7131.

(12) Bodák, B.; Maggioni, G. M.; Mazzotti, M. Effect of initial conditions on solid-state deracemization via temperature cycles: a model-based study. *Cryst. Growth Des.* **2019**, *19* (11), 6552−6559.

(13) Steendam, R. R.; van Benthem, T. J.; Huijs, E. M.; Meekes, H.; van Enckevort, W. J.; Raap, J.; Rutjes, F. P.; Vlieg, E. Deracemization controlled by reaction-induced nucleation: Viedma ripening as a

https://doi.org/10.1021/acsomega.4c06807
ACS Omega 2024, 9, 41936−41943

safety catch for total spontaneous resolution. *Cryst. Growth Des.* **2015**, *15* (8), 3917−3921.
(14) Steendam, R. R.; Ter Horst, J. H. Scaling Up Temperature Cycling-Induced Deracemization by Suppressing Nonstereoselective Processes. *Cryst. Growth Des.* **2018**, *18* (5), 3008−3015.
(15) Cameli, F.; Ter Horst, J. H.; Steendam, R. R. E.; Xiouras, C.; Stefanidis, G. D. On the effect of secondary nucleation on deracemization through temperature cycles. *Chem. - Eur. J.* **2020**, *26* (6), 1344−1354.
(16) Breveglieri, F.; Baglai, I.; Leeman, M.; Noorduin, W. L.; Kellogg, R. M.; Mazzotti, M. Performance analysis and model-free design of deracemization via temperature cycles. *Org. Process Res. Dev.* **2020**, *24* (8), 1515−1522.
(17) Spix, L.; Meekes, H.; Blaauw, R. H.; van Enckevort, W. J.; Vlieg, E. Complete deracemization of proteinogenic glutamic acid using viedma ripening on a metastable conglomerate. *Cryst. Growth Des.* **2012**, *12* (11), 5796−5799.
(18) Suwannasang, K.; Flood, A. E.; Rougeot, C.; Coquerel, G. Use of programmed damped temperature cycles for the deracemization of a racemic suspension of a conglomerate forming system. *Org. Process Res. Dev.* **2017**, *21* (4), 623−630.
(19) van der Meijden, M. W.; Leeman, M.; Gelens, E.; Noorduin, W. L.; Meekes, H.; van Enckevort, W. J.; Kaptein, B.; Vlieg, E.; Kellogg, R. M. Attrition-enhanced deracemization in the synthesis of clopidogrel-a practical application of a new discovery. *Org. Process Res. Dev.* **2009**, *13* (6), 1195−1198.
(20) Blessy, M.; Patel, R. D.; Prajapati, P. N.; Agrawal, Y. Development of forced degradation and stability indicating studies of drugs—A review. *J. Pharm. Anal.* **2014**, *4* (3), 159−165.
(21) Pal, K.; Yang, Y.; Nagy, Z. K. Model-based optimization of cooling crystallization of active pharmaceutical ingredients undergoing thermal degradation. *Cryst. Growth Des.* **2019**, *19* (6), 3417−3429.
(22) Intaraboonrod, K.; Harriehausen, I.; Carneiro, T.; Seidel-Morgenstern, A.; Lorenz, H.; Flood, A. E. Temperature Cycling Induced Deracemization of dl-Asparagine Monohydrate with Immobilized Amino Acid Racemase. *Cryst. Growth Des.* **2021**, *21* (1), 306−313.
(23) Wang, Y.; Sun, J.; Tang, W.; Gong, J. Green Chiral Separation of Racemic Mixture Via One-Step Crystallization Induced Deracemization Process Synergistically Intensified by Ultrasound and Temperature Cycling. *Chem. Eng. Sci.* **2023**, *281*, 119115.
(24) Fan, J.-P.; Tian, Z.-Y.; Tong, S.; Zhang, X.-H.; Xie, Y.-L.; Xu, R.; Qin, Y.; Li, L.; Zhu, J.-H.; Ouyang, X.-K. A novel molecularly imprinted polymer of the specific ionic liquid monomer for selective separation of synephrine from methanol−water media. *Food Chem.* **2013**, *141* (4), 3578−3585.
(25) Pellati, F.; Cannazza, G.; Benvenuti, S. Study on the racemization of synephrine by off-column chiral high-performance liquid chromatography. *J. Chromatogr. A* **2010**, *1217* (21), 3503−3510.
(26) Long, A. S.; Zhang, A. D.; Meyer, C. E.; Egilman, A. C.; Ross, J. S.; Wallach, J. D. Evaluation of trials comparing single-enantiomer drugs to their racemic precursors: A systematic review. *JAMA Network Open* **2021**, *4* (5), No. e215731.
(27) Kobayashi, Y.; Yato, M.; Ito, R.; Saito, K. Enantioselective determination of synephrine in health food products by liquid chromatography/time-of-flight mass spectrometry. *Chromatography* **2020**, *41* (1), 39−44.
(28) Zhang, Y.; Wang, S.; Luo, J.; Lin, Y.; Xu, X.; Han, C.; Kong, L. Preparative enantioseparation of synephrine by conventional and pH-zone-refining counter-current chromatography. *J. Chromatogr. A* **2018**, *1575*, 122−127.
(29) Rosa, F.; Négrier, P.; Corvis, Y.; Espeau, P. Crystal structure determination and thermal behavior upon melting of p-synephrine. *Thermochim. Acta* **2016**, *632*, 18−22.
(30) Ianno, V.; Clevers, S.; Negrier, P.; Dupray, V.; Coquerel, G.; Espeau, P. p-Synephrine enantiomers: binary phase diagram, crystal structure and kinetic stability of a metastable conglomerate monitored by nonlinear optics. *CrystEngcomm* **2020**, *22* (36), 6071−6080.
(31) Bergmann, E. D.; Sulzbacher, M. A new synthesis of 1-(m-and p-hydroxyphenyl)-2-methylaminoethanol (m-and p-sympathol). *J. Org. Chem.* **1951**, *16* (1), 84−89.
(32) Midgley, J. M.; Thonoor, C. M.; Drake, A. F.; Williams, C. M.; Koziol, A. E.; Palenik, G. J. The resolution and absolute configuration by X-ray crystallography of the isomeric octopamines and synephrines. *J. Chem. Soc., Perkin Trans. 2* **1989**, *8*, 963−969.
(33) Li, W. W.; Spix, L.; De Reus, S. C.; Meekes, H.; Kramer, H. J.; Vlieg, E.; Ter Horst, J. H. Deracemization of a racemic compound via its conglomerate-forming salt using temperature cycling. *Cryst. Growth Des.* **2016**, *16* (9), 5563−5570.
(34) Oketani, R.; Hoquante, M.; Brandel, C.; Cardinael, P.; Coquerel, G. Practical role of racemization rates in deracemization kinetics and process productivities. *Cryst. Growth Des.* **2018**, *18* (11), 6417−6420.
(35) Breveglieri, F.; Mazzotti, M. Role of racemization kinetics in the deracemization process via temperature cycles. *Cryst. Growth Des.* **2019**, *19* (6), 3551−3558.
(36) Mukhopadhyay, B.; Dattagupta, J. Crystal and molecular structure of 2, 2′-di-N-methylamino-1, 1′-di-p-hydroxyphenyldiethyleneether dihydrobromide,(C9H12ON· HBr) 2O. *J. Crystallogr. Spectrosc. Res.* **1988**, *18* (5), 509−516.
(37) Srisanga, S.; Ter Horst, J. H. Racemic compound, conglomerate, or solid solution: phase diagram screening of chiral compounds. *Cryst. Growth Des.* **2010**, *10* (4), 1808−1812.
(38) Sajid, M.; Anjum, S.; Choudhary, M. I.; Atta-ur-Rahman; Parvez, M.; Mohamed, I. E. Absolute configuration of (R)-synephrine hydrochloride. *Acta Crystallogr., Sect. E: Struct. Rep. Online* **2005**, *E61* (8), o2534−o2536.
(39) Xiouras, C.; Van Cleemput, E.; Kumpen, A.; Ter Horst, J. H.; Van Gerven, T.; Stefanidis, G. D. Towards deracemization in the absence of grinding through crystal transformation, ripening, and racemization. *Cryst. Growth Des.* **2017**, *17* (2), 882−890.
(40) Macrae, C. F.; Sovago, I.; Cottrell, S. J.; Galek, P. T. A.; McCabe, P.; Pidcock, E.; Platings, M.; Shields, G. P.; Stevens, J. S.; Towler, M.; et al. Mercury 4.0: From visualization to analysis, design and prediction. *J. Appl. Crystallogr.* **2020**, *53* (1), 226−235.
(41) Bourhis, L. J.; Dolomanov, O. V.; Gildea, R. J.; Howard, J. A.; Puschmann, H. The anatomy of a comprehensive constrained, restrained refinement program for the modern computing environment−Olex2 dissected. *Acta Crystallogr., Sect. A: Found. Adv.* **2015**, *71* (1), 59−75.
(42) Palatinus, L.; Prathapa, S. J.; Smaalen, S. V. EDMA: a computer program for topological analysis of discrete electron densities. *J. Appl. Crystallogr.* **2012**, *45* (3), 575−580.
(43) Sheldrick, G. M. Crystal structure refinement with SHELXL. *Acta Crystallogr., Sect. C: Struct. Chem.* **2015**, *71* (1), 3−8.
(44) Vishweshwar, P.; Nangia, A.; Lynch, V. M. Molecular complexes of homologous alkanedicarboxylic acids with isonicotinamide: X-ray crystal structures, hydrogen bond synthons, and melting point alternation. *Cryst. Growth Des.* **2003**, *3* (5), 783−790.
(45) Brünger, A. T. Free R value: a novel statistical quantity for assessing the accuracy of crystal structures. *Nature* **1992**, *355* (6359), 472−475.

https://doi.org/10.1021/acsomega.4c06807
ACS Omega 2024, 9, 41936−41943